

## Optical Trapping of High-Aspect-Ratio NaYF Hexagonal Prisms for kHz-MHz Gravitational Wave Detectors

George Winstone,<sup>1,\*</sup> Zhiyuan Wang,<sup>1,\*</sup> Shelby Klomp,<sup>1,\*</sup> Robert G. Felsted,<sup>2,\*</sup> Andrew Laeuger,<sup>1</sup> Chaman Gupta,<sup>3</sup> Daniel Grass,<sup>1</sup> Nancy Aggarwal,<sup>1,4</sup> Jacob Sprague,<sup>4</sup> Peter J. Pauzaskie,<sup>3,5</sup> Shane L. Larson,<sup>4</sup> Vicky Kalogera,<sup>4</sup> and Andrew A. Geraci<sup>1,4,†</sup>

(LSD Collaboration)

<sup>1</sup>*Center for Fundamental Physics, Department of Physics and Astronomy, Northwestern University, Evanston, Illinois 60208, USA*

<sup>2</sup>*Department of Chemistry, University of Washington, Seattle, Washington 98195, USA*

<sup>3</sup>*Department of Materials Science, University of Washington, Seattle, Washington 98195, USA*

<sup>4</sup>*Center for Interdisciplinary Exploration and Research in Astrophysics (CIERA), Department of Physics and Astronomy, Northwestern University, Evanston, Illinois 60208, USA*

<sup>5</sup>*Physical Sciences Division, Physical and Computational Sciences Directorate, Pacific Northwest National Laboratory, Richland, Washington 99352, USA*



(Received 26 April 2022; revised 23 June 2022; accepted 8 July 2022; published 28 July 2022)

We present experimental results on optical trapping of Yb-doped  $\beta$ -NaYF subwavelength-thickness high-aspect-ratio hexagonal prisms with a micron-scale radius. The prisms are trapped in vacuum using an optical standing wave, with the normal vector to their face oriented along the beam propagation direction, yielding much higher trapping frequencies than those typically achieved with microspheres of similar mass. This platelike geometry simultaneously enables trapping with low photon-recoil-heating, high mass, and high trap frequency, potentially leading to advances in high frequency gravitational wave searches in the Levitated Sensor Detector, currently under construction. The material used here has previously been shown to exhibit internal cooling via laser refrigeration when optically trapped and illuminated with light of suitable wavelength. Employing such laser refrigeration methods in the context of our work may enable higher trapping intensity and thus higher trap frequencies for gravitational wave searches approaching the several hundred kilohertz range.

DOI: [10.1103/PhysRevLett.129.053604](https://doi.org/10.1103/PhysRevLett.129.053604)

The field of levitated optomechanics is both rapidly developing and of high scientific interest, with a number of impressive recent results including achieving cooling to the quantum ground state [1,2], high resolution surface force mapping [3–5], material limited gigahertz rotations [6], microscopic material studies [7], and high precision force [8] and acceleration [9] sensitivity. Near term goals include contributions to dark matter and energy searches [10] and astrophysics, including searches for high frequency gravitational waves (GWs) in the Levitated Sensor Detector (LSD), currently under construction [11].

With the first detection of gravitational waves [12], there have been a number of proposed and constructed experimental efforts to extend the observable GW frequency spectrum, such as the upcoming LISA mission [13,14] and various other proposals [15–25]. Levitated sensors have been identified as a promising route to search for gravitational waves in the range of 10 kHz to a few hundred kilohertz [11,26], where sources can include GW emission from annihilation of axions in clouds around spinning black holes or from inspirals and mergers of nearby

sub-solar-mass primordial black holes within the Milky Way. In addition, a cosmological network of cosmic strings produces a stochastic background spanning frequencies from the nanohertz up to a cutoff well beyond the LSD band [27]. The sensitivity of such a levitated sensor detector benefits from low photon-recoil-heating and greater mass of the levitated particle. Both can be enabled by trapping disclike objects instead of spheres [11].

In this Letter, we demonstrate optical trapping and study the motional dynamics of high aspect ratio, high mass, high mechanical frequency hexagonal prisms in vacuum. We compare the measured motional spectra with simulations, and we illustrate the potential advances for high frequency gravitational wave detection made possible by trapping particles of this geometry. The main advance here is in achieving optical trapping and characterizing the dynamics of a dielectric object with a low-photon-recoil geometry while maintaining a large mass and high trapping frequency, which is essential for realizing the design sensitivity for the LSD gravitational wave search at frequencies above 10 kHz [11].

While small spherical particles can be trapped at high frequency ( $\sim 300$  kHz) [1,2], the near-isotropic nature of their light scattering yields significant photon recoil heating, and their low mass is undesirable for the application of GW detection. Larger diameter ( $\sim 10$   $\mu\text{m}$ ) spherical particles have significant mass, but have only been realized in subkilohertz-frequency trapping configurations [9,28]. The dislike geometry of high-aspect-ratio hexagonal prisms allows the ideal combination of high mass, high frequency, and low photon-recoil heating, and exhibits a clear improvement over levitated spheres, both in the regime when the sensor is dominated by thermal noise and when the sensor is limited by photon recoil. While these objects are of a lower mass than in our ideal design of LSD [11], this work represents a significant step along the technical roadmap and prepares us for trapping more customized similar objects in the final detector.

Since the first experimental demonstration of cold Brownian motion [29], solid-state laser refrigeration [30] has proven to be an effective way of preventing detrimental photothermal heating of optically levitated materials. In addition, NaYF and other rare-earth-doped crystals have been studied before in the context of optical vacuum levitation [31,32] and have been shown to exhibit laser refrigeration when trapped with light of an appropriate wavelength. Previous experiments with both cubic ( $\alpha$ ) and hexagonal ( $\beta$ ) phases of NaYF have either been with low mass subwavelength particles [32] or not optically levitated in vacuum [33]. By choosing such a material for the sensor, in the future laser refrigeration methods may enable higher trapping intensity and higher trap frequencies for gravitational wave searches approaching the several hundred kilohertz frequency range. To produce multimicrometer-scale high-aspect ratio particles relevant for GW detectors, we recently developed a novel hydrothermal synthesis [34] to drive growth of the hexagonal beta NaYF into thin, wide plates that was not previously possible [30].

Finally, as a general tool for precision sensing experiments, high aspect ratio trapped objects enable levitation of a multimicron scale object with mechanical frequencies in the tens of kilohertz, much higher than what is possible for similar mass spherical objects at similar optical powers [9,28], due to the subwavelength size of the object in the optical axis. Additionally,  $\beta$ -NaYF has a density roughly double that of  $\text{SiO}_2$ , further increasing the mass of the trapped particle. Because of common noise sources at lower frequencies, for example from ground vibration or acoustic noise, this is a useful experimental platform for measurements, e.g., accelerometry, that would benefit from a sensor with larger mass and higher bandwidth.

*Experimental setup.*—A top-view schematic of the experimental setup is shown in Fig. 1(a). Two focused counterpropagating linearly polarized Gaussian beams, which are obtained from a 1550 nm laser via polarization-maintaining fiber-optic couplers and circulators, create

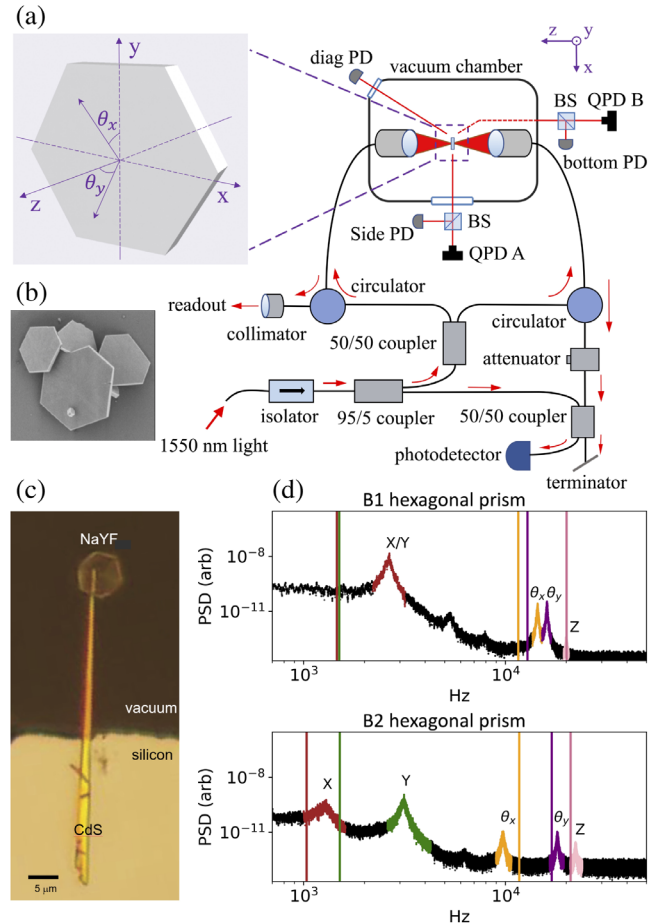


FIG. 1. (a) Setup. The hexagonal prism is trapped at the conjoined foci of two 1550 nm counterpropagating linearly polarized beams. Fiber-based detection is achieved through homodynelike interference of light coupled back into the polarization-maintaining fiber and the reference light out of the 95/5 coupler through a fiber photodetector (bandwidth of 1.6 GHz). Scattered light is also detected through a series of three biased photodiodes (PDs) and two quadrant photodetectors (QPDs) viewing the prism from the side, bottom, and top diagonal directions, as indicated. (b) Scanning electron beam micrograph of a cluster of NaYF hexagonal prisms from the B2 sample. (c) Optical micrograph of NaYF prism, adapted from Ref. [34]. (d) Spectral density of the motional signal at 2.2 mbar recorded by one of the QPD detectors for two different size hexagonal prisms, batch B1 (top  $P = 475$  mW) and B2 (bottom  $P = 250$  mW), respectively, with dimensions as described in the text. Motion corresponding to five principal degrees of freedom ( $x$ ,  $y$ ,  $z$ ,  $\theta_x$ ,  $\theta_y$ ) of the hexagon is visible, due to the nonperfectly orthogonal viewing angle of the detector. Vertical lines indicate calculated frequencies from a finite-element simulation for similar prisms, showing qualitative agreement.

a standing-wave optical dipole trap. Yb-doped  $\beta$ -NaYF hexagonal prisms are released from a glass substrate when driven by a piezoelectric transducer under 2–12 mbar of  $N_2$  gas [35] and trapped in one of the antinodes of the standing wave (total power at the trap  $P \approx 475$  mW, and beam waist

$w \approx 12 \mu\text{m}$ ). We study two batches  $B1$  and  $B2$ , with aspect ratios of approximately 8:1 ( $2.5 \mu\text{m}$  in diameter and  $300 \text{ nm}$  thick) and 15–25:1 ( $3\text{--}5 \mu\text{m}$  in diameter and  $200 \text{ nm}$  thick), respectively. The  $\beta$ -NaYF crystals are hydrothermally grown in an autoclave, resulting in a distribution of particle radii and thicknesses (see Supplemental Material [36]).

To characterize the motional dynamics of the prisms in the trap, we employed multiple independent detection mechanisms, as illustrated in Fig. 1(a). Light scattered from the prism is partially coupled back into the polarization-maintaining fiber and interferes with the reference light out of the 95/5 optical coupler to achieve homodynelike interferometric detection through a fiber photodetector. The image of the prism is projected onto two quadrant photodetectors from the side and bottom of the vacuum chamber, respectively. Additionally, scattered light is directly detected by three free-space biased photodiodes which view the prism from the side, bottom, and top diagonal windows of the chamber. Along the optical axis the positional information of the prism is encoded mainly in the phase of the light given the prism's subwavelength thickness in this direction. Off-axis positional information is encoded mainly in the intensity due to the much larger (a few micrometers) transverse dimensions of the prism.

*Theoretical model.*—Optical trapping of spheres in the Rayleigh, Mie-Lorentz and geometric optics regime is a fairly well studied problem experimentally and theoretically. Furthermore, several novel geometries have been explored in the subwavelength (Rayleigh) regime. The expected form for nonspherical objects optically trapped in the Mie-Lorentz regime is a topic of recent theoretical investigation [37]. While a sphere trapped in the Mie-Lorentz regime will exhibit 3 degrees of freedom, in contrast for a high-aspect-ratio radially symmetrically object (i.e., a disk or disk like object) we would expect to see 5 degrees of freedom, since the 6th degree of freedom (that of the hexagonal prism spinning around its most symmetrical axis) is poorly optically coupled. Our  $\beta$ -NaYF hexagons are neither perfectly symmetric nor optically isotropic so we would expect to see a coupling to the output light in the case that the rotations around that axis were driven. This could be explored in future experiments for example by using circularly polarized trapping light, since  $\beta$ -NaYF is birefringent.

Approximate, first-order solutions for a thin disc are given in [37]. The analytic approach predicts the mode ordering in frequency space that we observe, however, due to the non-infinitesimal thickness of the hexagonal prisms used in the experiment we use a finite element model implemented in PYGDM2 [38] to compute the expected optical forces and frequencies of the trapped prisms. Computed frequencies for our geometries are overlaid over experimental data in Fig. 1(d).

*Observed dynamics.*—Power spectral density data for the motion of two sizes of hexagonal prisms, lower aspect ratio  $B1$  and higher aspect ratio  $B2$ , trapped using  $475 \text{ mW}$  of

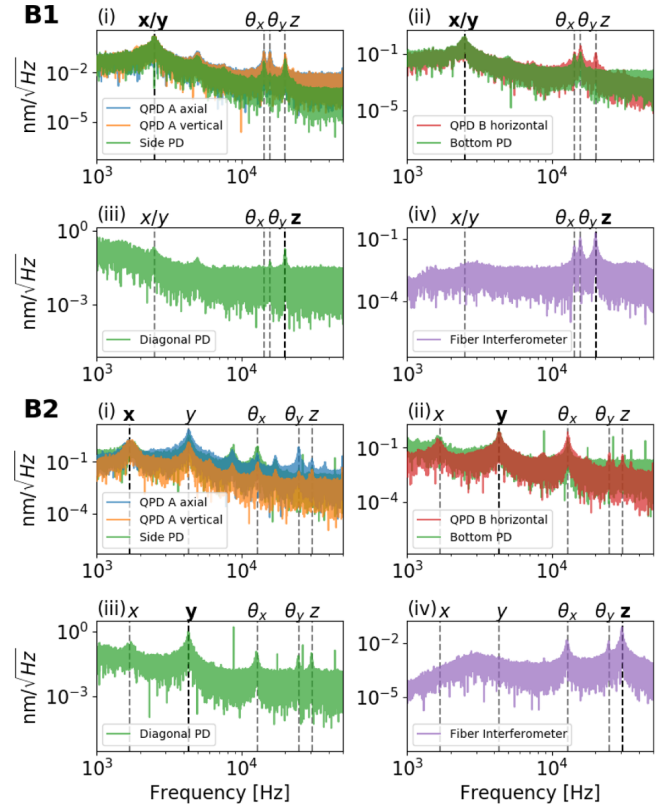


FIG. 2. Experimentally obtained power spectral densities for two sizes of hexagonal prisms,  $B1$  (top) and  $B2$  (bottom) from multiple detectors oriented to the side (i), bottom (ii), top diagonal (iii), and along the trap axis (iv). Detector types include quadrant photodetectors (blue, orange, and red), biased photodiodes (green), and a fiber-coupled homodynelike interferometric detector (purple). Observed peak maxima corresponding to  $x$ ,  $y$ ,  $\theta_x$ ,  $\theta_y$ , and  $z$  motion are denoted by vertical dashed lines. The  $x$  and  $y$  modes are degenerate for this  $B1$  prism. The vertical scale corresponds to the displacement in the direction used for detector calibration, as indicated also by the bold label (see Supplemental Material [36]). In some cases, higher harmonics of the labeled peaks are visible in the spectra, indicating the presence of nonlinearities.

laser power at a pressure of  $2.2 \text{ mbar}$  are shown in Fig. 2 for each of the detection mechanisms described previously. We pinpoint the mechanical resonances of the prisms by identifying peaks at same frequencies in multiple detectors. Peaks corresponding to primary translational and rotational mechanical resonances  $x$ ,  $y$ ,  $\theta_x$ ,  $\theta_y$ , and  $z$  are denoted by vertical dashed lines. All other peaks are identified as known harmonics, sidebands, or electronic noise in the system. The conversion to  $\text{nm}/\sqrt{\text{Hz}}$  is done for a harmonic trapping potential by assuming thermal equilibrium and fitting a strongly coupled peak to a Lorentzian function (see Supplemental Material [36]). The thermally driven torsional root-mean-squared amplitudes of the modes  $\theta_x$  and  $\theta_y$  can be estimated by the equipartition theorem:  $\theta_{x(y)} = (1/2\pi f_{\theta_{x(y)}}) \sqrt{(k_B T/I)}$ , where  $f_{\theta_{x(y)}}$  is the observed

torsional frequency,  $k_B$  is the Boltzmann constant,  $T$  is the temperature, and  $I$  is the moment of inertia. The calculated root-mean-square amplitudes of  $\theta_x$  and  $\theta_y$  are  $1.7 \times 10^{-2}$  rad and  $1.5 \times 10^{-2}$  rad, respectively, for  $B1$  and  $9.1 \times 10^{-3}$  rad and  $4.7 \times 10^{-3}$  rad for  $B2$ . We do not observe free rotations or bending modes, tested up to 10 MHz, as expected since the  $\theta_x$  and  $\theta_y$  modes of the prism are small amplitude, stable linear oscillatory modes about the plane of the standing wave's interference fringes and bending modes are not predicted to be observable within our resolution for this geometry. Since no free rotations are observed, we also do not observe the presence of a significant precession term as in Ref. [39].

*Mode splitting.*—The analytic model for a thin disc from Ref. [37] predicts a small amount of mode splitting along  $x/y$  and  $\theta_x/\theta_y$  axes, with the effect increasing the further the levitated object is from the Rayleigh regime—specifically in the radial axis. Therefore, a wider hexagonal prism will have a less degenerate set of  $x/y$  and  $\theta_x/\theta_y$  modes. This effect can be seen in both the outputs of the numerical model and the experimental data. Specifically in Fig. 2, the  $x/y$  modes for the radially smaller  $B1$  hexagon are nearly degenerate and the  $\theta_x/\theta_y$  modes are much closer together than for the radially larger  $B2$  hexagon. Mode splitting is also often seen in levitated particles in the Rayleigh limit, caused by the asymmetric potential generated by polarization dependent focusing of the beam [40]. Since our prisms are well into the Mie-Lorentz regime, separation between the modes results both from the polarization dependent focusing bias of the lens and geometry-dependent scattering resonances within the levitated particle [34].

*Finite element comparison.*—Figure 1(d) shows the power spectral density (PSD) of an optically trapped hexagonal prism with values from the finite element model (FEM) overlaid. The location of the peaks in the PSD is broadly in line with that computed by the FEM. It is of note that the frequency of the  $z$  degree of freedom is mainly dependent on the thickness of the hexagonal prism, while the mode splitting is mainly dependent on its radius. We assume the prism has uniform thickness, and surface roughness is not modelled. Differences in the observed frequency of the  $x/y$  motional modes to those predicted by the FEM may be driven by edge effects due to the prism's tapered shape (see Fig. S1 in Supplemental Material [36]). Because of memory and CPU time driven resolution constraints the FEM assumes a flat face on the hexagons prism's thin edge. Differences may also result due to geometry dependent Fabry-Perot and whispering gallery-mode-like resonances within the levitated prism [34].

*Sensitivity to gravitational waves.*—For the application of gravitational wave detection, a disc-shaped particle or hexagonal prism can be suspended in a standing wave in an optical cavity. For such a configuration, as discussed in Ref. [11], the minimum detectable strain  $h_{\text{limit}}$  for a particle with center-of-mass temperature  $T_{\text{CM}}$  is approximately

$$h_{\text{limit}} = \frac{4}{\omega_0^2 L} \sqrt{\frac{k_B T_{\text{CM}} \gamma_g b}{M}} \left[ 1 + \frac{\gamma_{\text{sc}}}{N_i \gamma_g} \right] H(\omega_0), \quad (1)$$

for a particle of mass  $M$  trapped in a cavity with response function  $H(\omega) \approx \sqrt{1 + 4\omega^2/\kappa^2}$  for a cavity of linewidth  $\kappa$ . Here  $N_i = k_B T_{\text{CM}}/\hbar\omega_0$ ,  $\gamma_g = (32P/\pi\bar{v}\rho t)$  is the gas damping rate at pressure  $P$  with mean gas speed  $\bar{v}$  for a plate or disc of thickness  $t$  and density  $\rho$ , and  $b$  is the bandwidth.

The photon recoil heating rate for a plate- or disc-shaped structure is [11,26,41]  $\gamma_{\text{sc}} = (V_c \lambda \omega_0/4L)[1/\int dV(\epsilon - 1)] \times (1/\mathcal{F}_{\text{disc}})$  is inversely proportional to the disc-limited finesse  $\mathcal{F}_{\text{disc}}$ , i.e.,  $2\pi$  divided by the fraction of photons scattered by the disc outside the cavity mode. The integral is performed over the extent of the suspended particle. Here  $V_c$  is the cavity mode volume [26]. For a subwavelength spherical particle of volume  $V$  in the Rayleigh regime,  $\gamma_{\text{sc}} = \frac{2}{5}(\pi^2 \omega_0 V/\lambda^3)[(\epsilon - 1)/(\epsilon + 2)]$ .

At higher pressure, the sensitivity is limited by gas collisions, while at ultrahigh vacuum,  $\gamma_{\text{sc}}/N_i \gamma_g > 1$  and eventually the sensitivity is limited by photon recoil heating. The thermal-noise limited sensitivity generally scales as  $\sqrt{P}$  in the gas-dominated, ballistic regime. At a given pressure, we can define a figure of merit  $\eta_{\text{thermal}}$  which describes the dependence on particle mass, geometry, and trapping frequency as  $\eta_{\text{thermal}} \equiv \omega_0^2 \sqrt{M \rho l}$ , where  $\omega_0$  is the trapping frequency along the cavity axis,  $l = r$  or  $l = t$  for spheres of radius  $r$  or plates of thickness  $t$ , respectively. Correspondingly, we define figure of merit  $\eta_{\text{recoil}} = \omega_0^{3/2} \sqrt{M/\gamma_{\text{sc}}}$  for sensitivity to GWs in the photon-recoil dominated limit.

In Fig. 3(b), we show  $\eta_{\text{thermal}}$  for several recent experimentally realized configurations. When comparing objects of similar mass, the higher frequencies obtained for our hexagonal prisms show a significant improvement. Although the values of  $\eta_{\text{thermal}}$  realized in the present work are only marginally better than those obtained for some of the smallest nanospheres trapped at very high frequencies (driven by the  $\omega_0^2$  scaling), by raising the trapping intensity we estimate for our geometry it should be possible to greatly exceed the highest values obtained in these experiments.

In ultrahigh vacuum, disk or hexagonal prism shaped objects show a distinct advantage, due to the more-directional nature of their scattering [as shown in Fig. 3(a)] in contrast to the nearly isotropic scattering from small spherical particles in the Rayleigh regime. In Fig. 3(b) we plot  $\eta_{\text{recoil}}$ , focusing on the higher frequency domain with a comparison between nanoparticles in the Rayleigh limit and hexagonal prisms of thickness 200 nm and diameter 5  $\mu\text{m}$ . The hexagonal prisms outperform the nanoparticles by 2 or more orders of magnitude for a disc-limited finesse of  $\mathcal{F}_{\text{disc}} = 10^5$ , reasonable for a suitably apodized disc or prism trapped in a beam with waist equal to half the particle radius [11,41]. For further GW sensitivity, a stacklike geometry (cf. Ref. [11]) may be

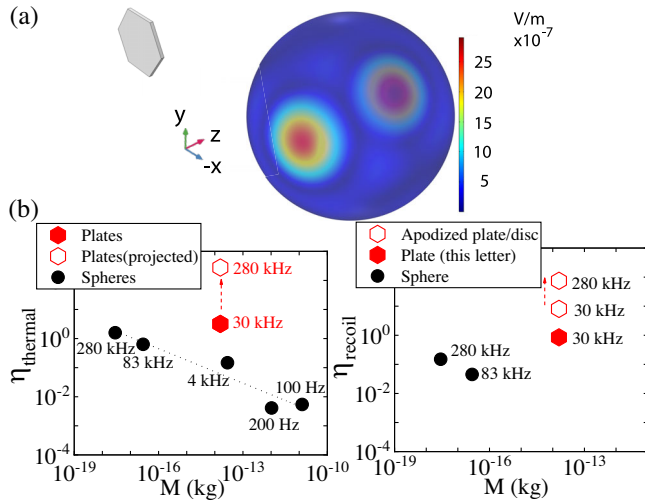


FIG. 3. (a) Calculated far-field scattered electric field profile  $|E|k$  for a hexagonal prism of thickness 200 nm and diameter  $4 \mu\text{m}$  (within the size range of the *B2* samples), for beam incident along  $x$  with a normalized electric field of 1 V/m. The color bar shows the magnitude of the field and the surface plot shows the directional dependence of scattering. (b) (left) Figure of merit  $\eta_{\text{thermal}} = \omega_0^2 \sqrt{M \rho l}$  (in units of  $\text{Hz}^2 \text{ kg/m}$ ) in the thermal-noise dominated limit, for spheres and plates of mass  $M$  and radius  $r = l$  or thickness  $t = l$ , respectively, for recent experimentally realized trapping configurations. At equal masses, high aspect ratio levitated plates (blue hexagons,  $5 \mu\text{m}$  diameter prism from sample *B2*) significantly outperform levitated spheres (black circles, as reported in Refs. [1,9,10,42,43], in order of decreasing frequency) for gravitational wave experiments due to their correspondingly higher trapping frequencies. Projected sensitivity for the same size plate held at higher trapping frequency is shown (open blue hexagon), as may be possible by using a higher intensity trap. (right) Figure of merit  $\eta_{\text{recoil}} = \omega_0^{3/2} \sqrt{M/\gamma_{\text{sc}}}$  (in units of  $\text{Hz kg}^{1/2}$ ) in the photon-recoil-heating dominated limit. Data for nanospheres from Refs. [1,42]. Projections shown for a prism of the size trapped in this work, for currently realized beam parameters with an estimated  $\mathcal{F}_{\text{disc}}$  of  $1.1 \times 10^3$  (solid hexagon) and for two trapping frequencies with a suitably apodized edge and beam waist profile, with an estimated  $\mathcal{F}_{\text{disc}}$  of  $10^5$  (open hexagons).

possible by using a central NaYF spacer and two end caps with high refractive index low-loss material such as Si or  $\text{Al}_2\text{O}_3$ , e.g., deposited by pulsed laser deposition [44] or evaporation.

**Conclusion.**—In conclusion, we present the first optical trapping of high aspect ratio Yb-doped  $\beta$ -NaYF hexagonal prisms, and compare the observed dynamics to a numerical model. For these prisms or other disc shaped sensors, the figure of merit  $\eta$  for sensitivity to gravitational waves significantly improves upon other spherical levitated systems both in the gas damping limited regime and the photon recoil heating limited regimes. NaYF has been shown in other experiments to exhibit anti-Stokes fluorescence cooling, when illuminated with light of a suitable wavelength.

Quasispherical nanocrystals with irregular morphologies prepared through top-down milling have also been cooled while being optically levitated [31]. Laser refrigeration of optically levitated disclike objects could allow higher trapping intensities and frequencies, yielding higher sensitivity to gravitational waves well above 100 kHz. Transferring these prisms, or objects of a similar geometry, into a Michelson-type 1 meter cavity instrument represents a next step in the technical road map of the Levitated Sensor Detector [11]. The successful trapping of these high aspect ratio hexagonal prisms therefore represents a significant step forward in developing  $> 10$  kHz gravitational wave astronomy.

We thank Francis Robicheaux and Marko Toros for insightful discussions on the equations of motion for the disks. A. G., G. W., and N. A. are supported in part by NSF Grant No. 2110524, the Heising-Simons Foundation, the John Templeton Foundation, and ONR Grant No. N00014-18-1-2370. A. G. and S. L. are supported by the W. M. Keck Foundation. V. K. is supported by a CIFAR Senior Fellowship and through Northwestern University through the D. I. Linzer Distinguished University Professorship. N. A. is also supported by the CIERA Postdoctoral Fellowship from the Center for Interdisciplinary Exploration and Research in Astrophysics at Northwestern University. This work used KyRIC (Kentucky Research Informatics Cloud) through the Extreme Science and Engineering Discovery Environment (XSEDE) with allocation TG-PHY210012, and the Quest computing facility at Northwestern.

\*These authors contributed equally to this work.

†Corresponding author.

andrew.geraci@northwestern.edu

- [1] U. Delić, M. Reisenbauer, K. Dare, D. Grass, V. Vuletić, N. Kiesel, and M. Aspelmeyer, Cooling of a levitated nanoparticle to the motional quantum ground state, *Science* **367**, 892 (2020).
- [2] F. Tebbenjohanns, M. L. Mattana, M. Rossi, M. Frimmer, and L. Novotny, Quantum control of a nanoparticle optically levitated in cryogenic free space, *Nature (London)* **595**, 378 (2021).
- [3] C. P. Blakemore, A. D. Rider, S. Roy, Q. Wang, A. Kawasaki, and G. Gratta, Three-dimensional force-field microscopy with optically levitated microspheres, *Phys. Rev. A* **99**, 023816 (2019).
- [4] C. Montoya, E. Alejandro, W. Eom, D. Grass, N. Clarisse, A. Witherspoon, and A. A. Geraci, Scanning force sensing at micrometer distances from a conductive surface with nanospheres in an optical lattice, *Appl. Opt.* **61**, 3486 (2022).
- [5] G. Winstone, R. Bennett, M. Rademacher, M. Rashid, S. Buhmann, and H. Ulbricht, Direct measurement of the electrostatic image force of a levitated charged nanoparticle close to a surface, *Phys. Rev. A* **98**, 053831 (2018).

- [6] R. Reimann, M. Doderer, E. Hebestreit, R. Diehl, M. Frimmer, D. Windey, F. Tebbenjohanns, and L. Novotny, Ghz Rotation of an Optically Trapped Nanoparticle in Vacuum, *Phys. Rev. Lett.* **121**, 033602 (2018).
- [7] F. Ricci, M. T. Cuairan, A. W. Schell, E. Hebestreit, R. A. Rica, N. Meyer, and R. Quidant, A chemical nano-reactor based on a levitated nanoparticle in vacuum, [arXiv:2107.01084](https://arxiv.org/abs/2107.01084).
- [8] G. Ranjit, M. Cunningham, K. Casey, and A. A. Geraci, Zeptonewton force sensing with nanospheres in an optical lattice, *Phys. Rev. A* **93**, 053801 (2016).
- [9] F. Monteiro, S. Ghosh, A. G. Fine, and D. C. Moore, Optical levitation of 10-ng spheres with nano- $g$  acceleration sensitivity, *Phys. Rev. A* **96**, 063841 (2017).
- [10] F. Monteiro, G. Afek, D. Carney, G. Krnjaic, J. Wang, and D. C. Moore, Search for Composite Dark Matter with Optically Levitated Sensors, *Phys. Rev. Lett.* **125**, 181102 (2020).
- [11] N. Aggarwal, G. P. Winstone, M. Teo, M. Baryakhtar, S. L. Larson, V. Kalogera, and A. A. Geraci, Searching for New Physics with a Levitated-Sensor-Based Gravitational-Wave Detector, *Phys. Rev. Lett.* **128**, 111101 (2022).
- [12] B. P. Abbott *et al.*, Observation of Gravitational Waves from a Binary Black Hole Merger, *Phys. Rev. Lett.* **116**, 061102 (2016).
- [13] P. A. Seoane *et al.* (eLISA Collaboration), The gravitational universe, [arXiv:1305.5720](https://arxiv.org/abs/1305.5720).
- [14] P. Amaro-Seoane *et al.*, Laser interferometer space antenna, [arXiv:1702.00786](https://arxiv.org/abs/1702.00786).
- [15] S. Kolkowitz, I. Pikovski, N. Langellier, M. D. Lukin, R. L. Walsworth, and J. Ye, Gravitational wave detection with optical lattice atomic clocks, *Phys. Rev. D* **94**, 124043 (2016).
- [16] J. Coleman (MAGIS-100 Collaboration), Matter-wave atomic gradiometer interferometric sensor (MAGIS-100) at Fermilab, *Proc. Sci.*, ICHEP2018 (2019) 021 [[arXiv:1812.00482](https://arxiv.org/abs/1812.00482)].
- [17] A. S. Chou, R. Gustafson, C. Hogan, B. Kamai, O. Kwon, R. Lanza, S. L. Larson, L. McCuller, S. S. Meyer, J. Richardson, C. Stoughton, R. Tomlin, and R. Weiss (Holometer Collaboration), MHz gravitational wave constraints with decameter Michelson interferometers, *Phys. Rev. D* **95**, 063002 (2017).
- [18] T. Akutsu *et al.*, Search for a Stochastic Background of 100-MHz Gravitational Waves with Laser Interferometers, *Phys. Rev. Lett.* **101**, 101101 (2008).
- [19] V. Domcke and C. Garcia-Cely, Potential of Radio Telescopes as High-Frequency Gravitational Wave Detectors, *Phys. Rev. Lett.* **126**, 021104 (2021).
- [20] S. Singh, L. A. De Lorenzo, I. Pikovski, and K. C. Schwab, Detecting continuous gravitational waves with superfluid  $^4\text{He}$ , *New J. Phys.* **19**, 073023 (2017).
- [21] A. Cruise, The potential for very high-frequency gravitational wave detection, *Classical Quantum Gravity* **29**, 095003 (2012).
- [22] S. M. Vermeulen, L. Aiello, A. Ejlli, W. L. Griffiths, A. L. James, K. L. Dooley, and H. Grote, An experiment for observing quantum gravity phenomena using twin table-top 3D interferometers, *Classical Quantum Gravity* **38**, 085008 (2021).
- [23] A. Nishizawa, S. Kawamura, T. Akutsu, K. Arai, K. Yamamoto, D. Tatsumi, E. Nishida, M.-a. Sakagami, T. Chiba, R. Takahashi *et al.*, Laser-interferometric detectors for gravitational wave backgrounds at 100 MHz: Detector design and sensitivity, *Phys. Rev. D* **77**, 022002 (2008).
- [24] A. Ito, T. Ikeda, K. Miuchi, and J. Soda, Probing GHz gravitational waves with graviton-magnon resonance, *Eur. Phys. J. C* **80**, 1 (2020).
- [25] A. Ejlli, D. Ejlli, A. M. Cruise, G. Pisano, and H. Grote, Upper limits on the amplitude of ultra-high-frequency gravitational waves from graviton to photon conversion, *Eur. Phys. J. C* **79**, 1 (2019).
- [26] A. Arvanitaki and A. A. Geraci, Detecting High-Frequency Gravitational Waves with Optically Levitated Sensors, *Phys. Rev. Lett.* **110**, 071105 (2013).
- [27] P. Binétruy, A. Bohé, C. Caprini, and J.-F. Dufaux, Cosmological backgrounds of gravitational waves and eLISA/NGO: Phase transitions, cosmic strings and other sources, *J. Cosmol. Astropart. Phys.* **06** (2012) 027.
- [28] A. D. Rider, D. C. Moore, C. P. Blakemore, M. Louis, M. Lu, and G. Gratta, Search for Screened Interactions Associated with Dark Energy below the 100  $\mu\text{m}$  Length Scale, *Phys. Rev. Lett.* **117**, 101101 (2016).
- [29] P. B. Roder, B. E. Smith, X. Zhou, M. J. Crane, and P. J. Pauzauskie, Laser refrigeration of hydrothermal nanocrystals in physiological media, *Proc. Natl. Acad. Sci. U.S.A.* **112**, 15024 (2015).
- [30] X. Xia, A. Pant, X. Zhou, E. A. Dobretsova, A. B. Bard, M. B. Lim, J. Y. D. Roh, D. R. Gamelin, and P. J. Pauzauskie, Hydrothermal synthesis and solid-state laser refrigeration of ytterbium-doped potassium-lutetium-fluoride (KLF) microcrystals, *Chem. Mater.* **33**, 4417 (2021).
- [31] A. T. M. A. Rahman and P. F. Barker, Laser refrigeration, alignment and rotation of levitated  $\text{Yb}^{3+}$ : YLF nanocrystals, *Nat. Photonics* **11**, 634 (2017).
- [32] D. R. Luntz-Martin, R. G. Felsted, S. Dadras, P. J. Pauzauskie, and A. N. Vamivakas, Laser refrigeration of optically levitated sodium yttrium fluoride nanocrystals, *Opt. Lett.* **46**, 3797 (2021).
- [33] X. Zhou, B. E. Smith, P. B. Roder, and P. J. Pauzauskie, Laser refrigeration of ytterbium-doped sodium-yttrium-fluoride nanowires, *Adv. Mater.* **28**, 8658 (2016).
- [34] R. Felsted, A. Pant, A. Bard, X. Xia, D. Luntz-Martin, S. Dadras, Siamak, Zhang, A. Vamivakas, and P. Pauzauskie, Chemically tunable aspect ratio control and laser refrigeration of hexagonal sodium yttrium fluoride upconverting materials, *Cryst. Growth Des.* **22**, 3605 (2022).
- [35] M. Beck, Overcoming “Stiction” Forces: Launching Silica Microspheres into an Optical Trap, Senior Thesis, University of Nevada, Reno, 2012.
- [36] See Supplemental Material at <http://link.aps.org/supplemental/10.1103/PhysRevLett.129.053604> for further details on prism fabrication, mechanical mode characterization, and detector displacement calibration.
- [37] T. Seberson and F. Robicieux, Stability and dynamics of optically levitated dielectric disks in a Gaussian standing wave beyond the harmonic approximation, *Phys. Rev. Research* **2**, 033437 (2020).

- [38] P. R. Wiecha, PYGDM-A PYTHON toolkit for full-field electro-dynamical simulations and evolutionary optimization of nanostructures, *Comput. Phys. Commun.* **233**, 167 (2018).
- [39] M. Rashid, M. Toroš, A. Setter, and H. Ulbricht, Precession Motion in Levitated Optomechanics, *Phys. Rev. Lett.* **121**, 253601 (2018).
- [40] L. Novotny and B. Hecht, *Principles of Nano-Optics* (Cambridge University Press, Cambridge, England, 2012).
- [41] D. E. Chang, K.-K. Ni, O. Painter, and H. J. Kimble, Ultrahigh-Q mechanical oscillators through optical trapping, *New J. Phys.* **14**, 045002 (2012).
- [42] C. R. Harvey, E. Weisman, C. Galla *et al.*, Nanomechanical testing of silica nanospheres for levitated optomechanics experiments (to be published).
- [43] G. Ranjit, D. P. Atherton, J. H. Stutz, M. Cunningham, and A. A. Geraci, Attonewton force detection using microspheres in a dual-beam optical trap in high vacuum, *Phys. Rev. A* **91**, 051805(R) (2015).
- [44] R. Boidin, T. Halenkovic, V. Nazabal, L. Benes, and P. Nemeč, Pulsed laser deposited alumina thin films, *Ceram. Int.* **42**, 1177 (2016).